Microstructural and dielectric properties of donor doped (La^{3+}) CaCu$_3$Ti$_4$O$_{12}$ ceramics

B. Shri Prakash · K. B. R. Varma

Abstract The effect of La^{3+} doping on Ca^{2+} sites in CaCu$_3$Ti$_4$O$_{12}$ (CCTO) was examined. Polycrystalline samples in the chemical formula Ca$_{(1-x)}$La$_{(2/3)x}$Cu$_3$Ti$_4$O$_{12}$ with x = 0, 0.5, 1 were synthesized via the conventional solid state reaction route. X-ray powder diffraction analysis confirmed the formation of the monophasic compounds and indicated the structure to be remaining cubic with a small increase in lattice parameter with increase in La^{3+} doping. The dielectric and impedance characteristics of Ca$_{(1-x)}$La$_{(2/3)x}$Cu$_3$Ti$_4$O$_{12}$ were studied in the 100 Hz–10 MHz frequency range at various temperatures (100–475 K). A remarkable decrease in grain size from 50 μm to 3–5 μm was observed on La^{3+} substitution. The dielectric constant of CaCu$_3$Ti$_4$O$_{12}$ decreased drastically on La^{3+} doping. The frequency and temperature responses of dielectric constant of La^{3+} doped samples were found to be similar to that of CaCu$_3$Ti$_4$O$_{12}$. The effects of La^{3+} doping on the electrical properties of CaCu$_3$Ti$_4$O$_{12}$ were probed using impedance spectroscopy. The conducting properties of grain decreased while that of the grain boundary increased on La^{3+} doping, resulting in a decrease of the internal barrier layer effect. A decrease in grain boundary capacitance and stable grain response in La^{3+} doped CCTO ceramics were unambiguously established by modulus spectra studies.

B. Shri Prakash (✉) · K. B. R. Varma
Materials Research Centre, Indian Institute of Science, Bangalore 560012, India
e-mail: spb@mrc.iisc.ernet.in

1 Introduction

Electroceramics associated with giant dielectric constants accompanied by low loss have been in increasing demand owing to their potential use in miniaturized active/passive devices [1–5]. The conspicuously high dielectric constant that was reported for Centro symmetric perovskite related calcium copper titanate (CaCu$_3$Ti$_4$O$_{12}$) ceramics has drawn the attention of many researchers around the globe [6–17]. The dielectric constant measurements that were carried out on both ceramics and single crystals over wide frequency and temperature ranges revealed the existence of giant dielectric constant. Impedance spectroscopic data obtained on CaCu$_3$Ti$_4$O$_{12}$ (CCTO) ceramics demonstrated their electrical heterogeneous character and large dielectric constant was attributed to a grain boundary barrier layer capacitance effects [8, 9, 14]. Transmission electron microscopic investigations unraveled an important role played by the grain boundaries in the electrical transport properties of CCTO [18]. In order to have an insight into the possible strong microstructure property correlations, several attempts were made to fabricate these ceramics with varied grain sizes and grain boundary layer thicknesses. In addition, it is known in the literature that, the donor/acceptor dopants, dopant mechanisms and the conditions under which the ceramics are processed would influence the physical properties of, particularly perovskite related electroceramics [19–21]. It was felt that, it would be interesting to visualize the influence of rare earths oxide doping on the microstructural and dielectric properties of CCTO ceramics. To begin with, the studies concerning the effect of La^{3+} doping (on calcium site) on the above mentioned
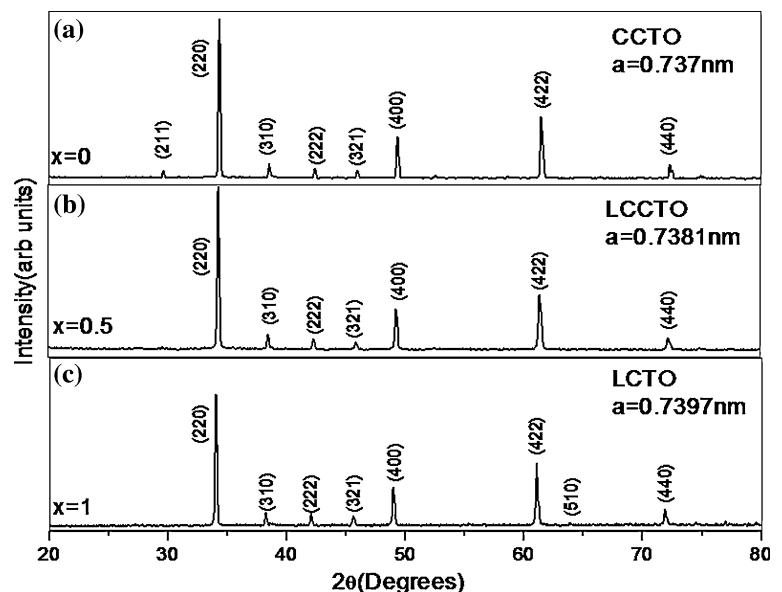
characteristics of CCTO ceramics have been taken up. Albeit, the effect of replacement of Ca^{2+} by donor dopant (Lanthanum (La^{3+})) was reported in the literature, the details with regard to the microstructure–property correlation are obscure [7, 22]. In this paper, we report the effect of lanthanum doping on the microstructure, dielectric, impedance and modulus characteristics of CCTO ceramics.

2 Experimental

Polycrystalline powder samples of $Ca_{(1-x)}La_{(2/3)x}Cu_3Ti_4O_{12}$ in which $x = 0.5$ (LCCTO) and $x = 1$ (LCTO) along with $x = 0$ (CCTO) were synthesized using the stoichiometric amounts of $CaCO_3$, La_2O_3, CuO and TiO_2 (> 99% purity). These were thoroughly mixed in an acetone medium using a ball mill. Subsequently these mixtures were oven dried for about 2 h. This was followed by the calcination of the powder in Alumina crucible at 1000–1025°C temperature range with intermittent grinding for 10 h. The crystalline phase formation of the calcined powder was confirmed via X-ray powder diffraction (XRD) technique using Philips X-ray diffractometer. The calcined powder so obtained was cold pressed into the cylindrical pellets of diameter 10 mm and thickness of about 2 mm using PVA as binder. All the pellets were sintered in an air at 1075°C for 10 h and fine polished with emery paper to make their faces flat and parallel. These were polished to the same thickness, so as to avoid the ambiguities related to the dimensionalities. The densities of the sintered pellets were determined by Archimedean principle using Xylene as the liquid medium.

The microstructural features and grain size distribution in sintered pellets were studied by scanning electron microscopy (SEM) (S360, Cambridge Instruments) and the elemental analysis was carried out using the EDX associated with the SEM.

The capacitance and impedance measurements were carried out as a function of frequency (100 Hz–10 MHz) and temperature (100–475 K), using impedance gain phase analyzer (HP4194A) at signal strength of 0.5 V_{rms}. For this, gold electrodes were sputtered on CCTO pellets and Copper leads were glued to these electrodes using silver paste.

3 Results and discussion

3.1 Structural and microstructural analyses

The XRD patterns that were obtained for all the three powdered samples viz. $x = 0$ (CCTO), $x = 0.5$ (LCCTO) and $x = 1$ (LCTO) in the chemical formula $Ca_{(1-x)}La_{(2/3)x}Cu_3Ti_4O_{12}$ are shown in the Fig. 1(a–c). The pattern for $x = 0$ is in good agreement with the one reported for CCTO in the literature [7]. The doping of La^{3+} on Ca^{2+} sites in CCTO has resulted in a small shift towards lower 2θ in the X-ray Bragg peak positions. However, the X-ray structure remains to be cubic. Nevertheless, there is an increase in the lattice parameter from $a = 7.37$–7.397 Å, which is attributed to the ionic size effects (as La^{3+} is bigger than Ca^{2+}).

Figure 2(a and b) shows the scanning electron micrographs recorded for the thermally etched (1025°C) CCTO and LCTO ceramics. The one obtained for CCTO ceramics (Fig. 2a) revealed the
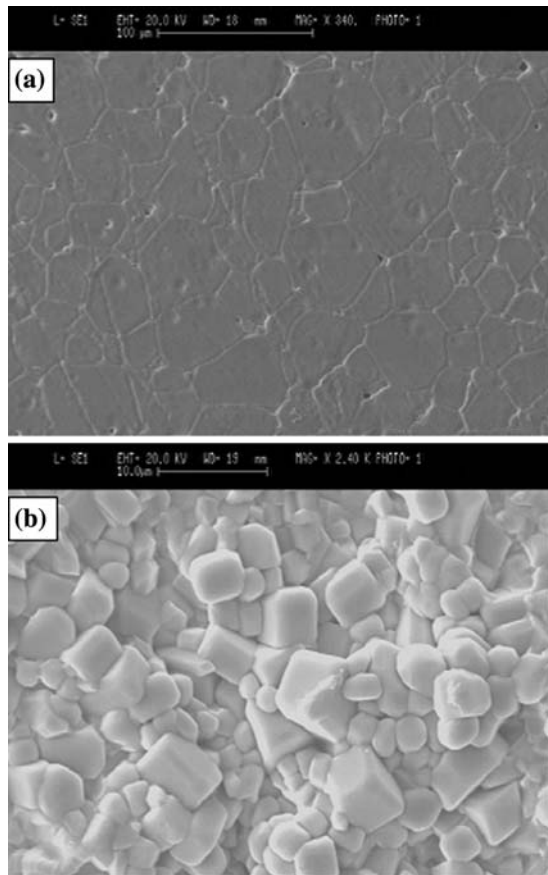
Fig. 1 X-ray powder diffraction patterns for (**a**) $x = 0$ (CCTO), (**b**) $x = 0.5$ (LCCTO), (**c**) $x = 1$ (LCTO) of $Ca_{(1-x)}La_{(2/3)x}Cu_3Ti_4O_{12}$ ceramics

Fig. 2 Scanning electron micrographs of $Ca_{(1-x)}La_{(2/3)x}Cu_3Ti_4O_{12}$ ceramics for (**a**) $x = 0$ (CCTO), (**b**) $x = 1$ (LCTO)

presence of abnormally large grains with an average grain size of about 50 μm. La^{3+} substitution for Ca^{2+} in CCTO has resulted in a remarkable decrease in grain size from 50 μm to 3–5 μm (Fig. 2b). In addition, CCTO consists of Cu rich phase at the grain boundaries in contrast with almost homogeneous composition in the case of LCTO as confirmed via EDX analyses. Further, the grains of LCTO have smooth surfaces associated with a squarish appearance. The influence of above features has been visualized by monitoring the electrical transport properties of CCTO, LCCTO and LCTO ceramics. The details of which are elucidated in the following sections.

3.2 Dielectric studies

The variation of the real (ε_r') and imaginary parts (ε_r'') of the dielectric constant with frequency at various temperatures (110–250 K) for LCTO is shown in Fig. 3(a and b). ε_r' exhibits Debye-like relaxation and shifts to higher frequency on increasing the temperature. Indeed, it is very much evident in the ε_r'' behavior and the peak shifts to higher frequency with increasing temperature as in the case of CCTO [1, 8]. The ε_r' value at 100 kHz and 300 K for LCTO is about 1700, which is much higher than the one reported (418) in the literature [7]. The higher ε_r' value that is obtained in the present studies is attributed to the difference in micro structural aspects. It is known in the literature that a

Fig. 3 Frequency dependence of constant ε^* at different temperatures. (**a**) Real part (ε_r'), (**b**) imaginary part (ε_r'') for $x = 1$ in $Ca_{(1-x)}La_{(2/3)x}Cu_3Ti_4O_{12}$ ceramics (LCTO)
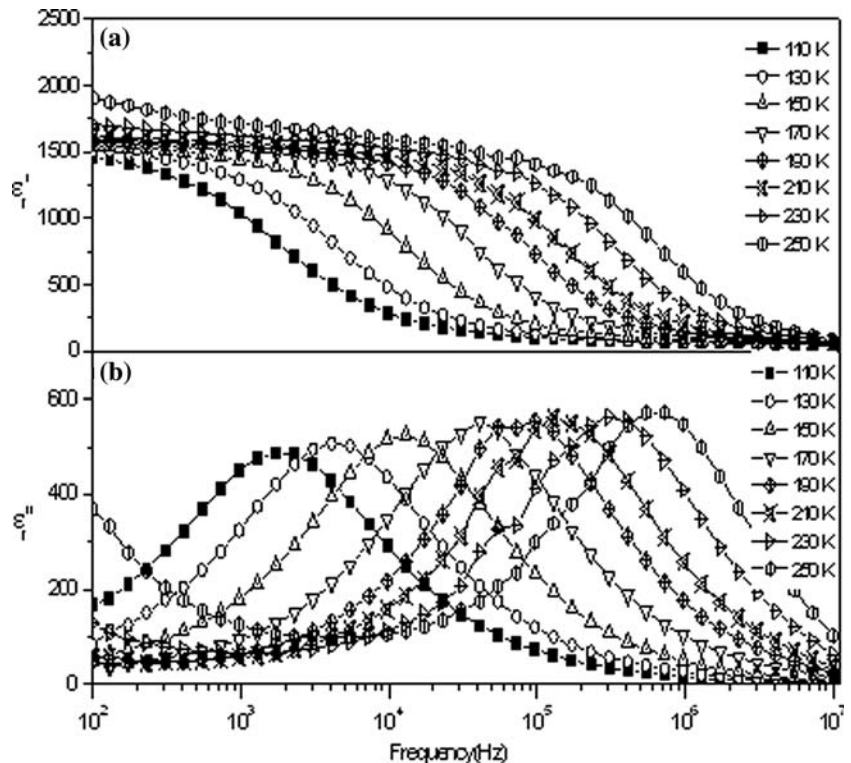
subtle change in the processing conditions would result in a large variation in the dielectric constant of CCTO ceramics [12, 23].

The temperature (100–400 K) dependence of ε_r' and ε_r'' for LCTO at different frequencies is shown in Fig. 4(a and b). ε_r' shows a sudden rise from about 100 to 1500 when the temperature is changed from 100 to 175 K at 10 kHz as shown in Fig. 4a. Subsequently, it levels of up to about 300 K and starts rising steeply up to the temperature (475 K) that is covered in the present studies. This behavior seems to have strong frequency dependence, as it does not behave in the same manner at high frequencies. The sudden rise in ε_r' is accompanied by a peak in ε_r'' which shifts to a higher temperature with increasing frequency.

In order to depict the difference in the variation of ε_r' between CCTO, LCCTO and LCTO especially at low frequencies, frequency dependence of ε_r' for these compounds have been plotted at two representative temperatures 120 and 300 K (Fig. 5 (a and b)). The dielectric relaxation that is encountered around 10^4 Hz at 120 K in all the samples shifts towards higher frequencies at 300 K. It is clear from the Fig. 5b that the low frequency dielectric constant of CCTO is nearly 10 times larger than that of LCTO. LCCTO has the dielectric constant almost twice that of LCTO in the low frequency region. It is interesting to note from Fig. 5a that, the high frequency dielectric response, which is likely to originate from the lattice, is nearly the same for all the three compounds covered in the present studies and its value is around 80 at 1 MHz.

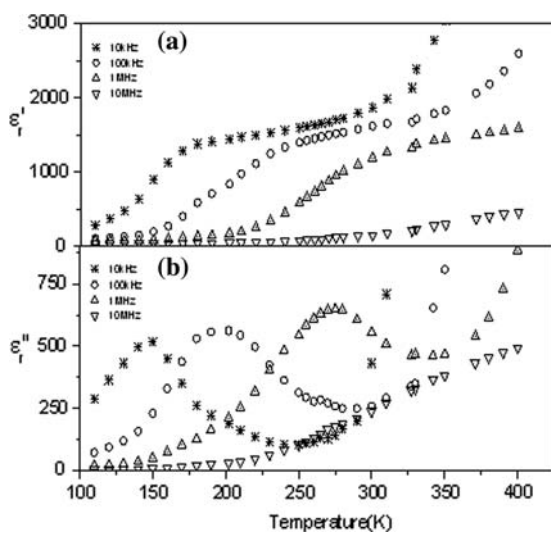Though, there are different views regarding the very origin of large ε_r' at low frequencies in CCTO ceramics,

Fig. 5 Frequency dependence of real part of dielectric constant ε_r' of $Ca_{(1-x)}La_{(2/3)x}Cu_3Ti_4O_{12}$ ceramics with $x = 0$ (CCTO), $x = 0.5$ (LCCTO), $x = 1$ (LCTO) at two different temperatures (**a**) 120 K, (**b**) 300 K

it is implicit that it has mostly extrinsic origin. Therefore, it would be interesting to probe all the samples under study with complex impedance spectroscopy (IS) in view of its capability to correlate electrical behavior of the sample to its microstructure.

3.3 Complex impedance analysis

The resistance and capacitance associated with an electrically active grain and the grain boundary regions in electroceramics could be estimated by IS. Impedance data could often be modeled by an equivalent circuit consisting of two parallel RC elements connected in series as shown in the Fig. 6; one representing to the grain effects and other representing the grain boundary response. For such a circuit, each RC
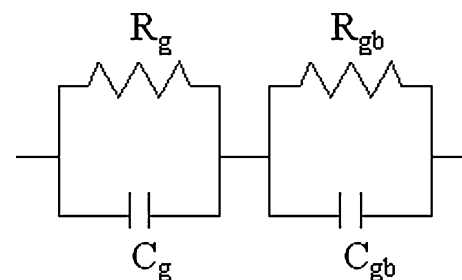

Fig. 4 Temperature dependence of dielectric constant ε^* at different frequencies. (**a**) Real part (ε_r'), (**b**) imaginary part (ε_r'') for $x = 1$ in $Ca_{(1-x)}La_{(2/3)x}Cu_3Ti_4O_{12}$ ceramics (LCTO)

Fig. 6 Equivalent circuit used to represent the electrical properties of the grain and grain boundary effects

element ideally gives rise to semicircular arc in complex impedance plane Z^* [24], where

$$Z^* = Z' - iZ''$$

where

$$Z' = \frac{R_g}{1 + (\omega R_g C_g)^2} + \frac{R_{gb}}{1 + (\omega R_{gb} C_{gb})^2}$$

and

$$Z'' = R_g\left[\frac{\omega R_g C_g}{1 + (\omega R_g C_g)^2}\right] + R_{gb}\left[\frac{\omega R_{gb} C_{gb}}{1 + (\omega R_{gb} C_{gb})^2}\right]$$

R_g, R_{gb} and C_g, C_{gb} are the resistances and capacitances of grains and grain boundaries, respectively.

Figure 7a shows the Z^* (Z' versus Z'') plots for CCTO at three different temperatures (110, 120, 130 K). It yielded semicircles with their high frequency ends passing through the origin and large spikes appear at the low frequency end. The semicircle shrinks with increasing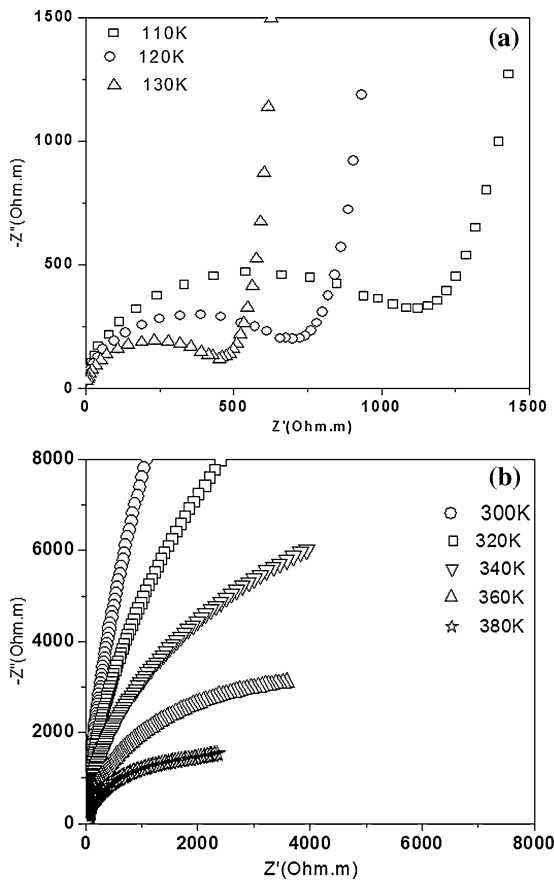 temperature. This behavior is consistent with that reported in the literature for CCTO at low temperature and the semicircle has been attributed to the grain response [8].

The Z^* plots for CCTO at room temperature and above are shown in Fig. 7b. It comprises of large arc with nonzero intercept at high frequencies. The appearance of the semicircle becomes clearer at higher temperatures (380 K). This high temperature semicircle is ascribed to the high resistive grain boundary with high frequency intercept value corresponding to the grain resistance at a temperature under measurement [8].

Resistances of the grain and grain boundary could be evaluated from the diameters of low and high temperature semicircles. These values suggest that grain boundary resistance is much larger than the grain resistance. Conductivity (σ), where $\sigma = R^{-1}$, was obtained for the bulk, (σ_b), and grain boundary, (σ_{gb}), components and plotted against reciprocal temperatures in Fig. 8(a and b). Both obeyed the Arhenius law with activation energies of 0.062 and 0.70 eV, respectively. While, these are in agreement with the reported values in general for CCTO, the grain boundary activation energy is slightly higher than that reported in the literature [8]. The activation energy associated with the grains is suggestive of their semiconductive nature. The semiconductivity of CCTO grains is reported to be originating from oxygen loss during the ceramic processing in air at elevated temperatures [8]. The grain resistances obtained from high frequency intercept
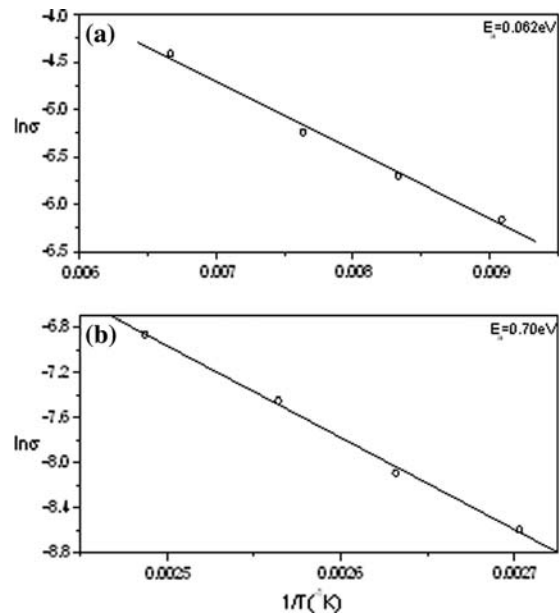

Fig. 7 Impedance complex plane plot, Z^* of CCTO ceramics at (a) low temperatures, (b) above room temperature

Fig. 8 Arhenius plot for (a) bulk and (b) grain boundry conductivity for CCTO ceramics
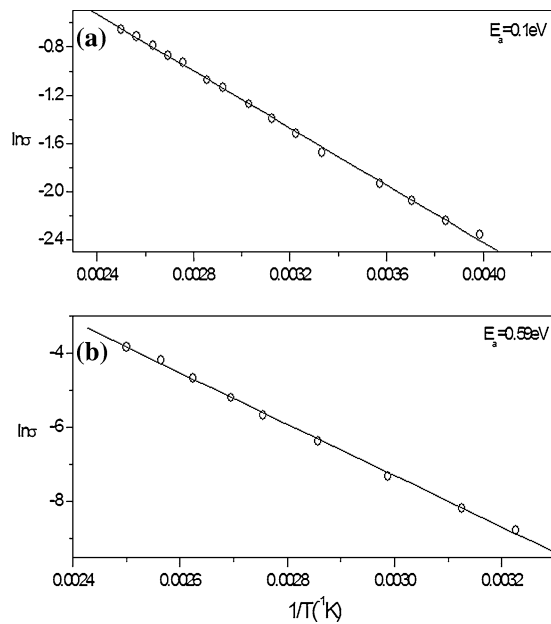
Fig. 9 Arhenius plot for (**a**) bulk and (**b**) grain boundry conductivity for LCTO ceramics

values are also used to calculate grain activation energy. The activation energy so obtained is equal to the one obtained from the diameter of the semicircle at lower temperatures. This equality suggests that the grain activation energy could be calculated from its resistance obtained either from low temperature semicircles or high temperature high frequency intercepts.

LCCTO and LCTO ceramics were also analyzed by Impedance spectroscopy. Grain and grain boundary responses of these fall into two separate temperature regimes akin to that of CCTO. Low temperature regions were dominated by grain response and the grain boundary responses appear above room temperature. The grain and grain boundary activation energies of LCTO were calculated by considering the $\sigma = R^{-1}$ and their variation with temperature. Both the regions obey the Arhenius law associated with the activation energies of 0.1 and 0.59 eV, respectively as shown in Fig. 9. It should be noted that the activation energy thus obtained for LCTO grains nearly twice that of the CCTO grain and the grain boundary activation energy is slightly less than that of CCTO.

Figure 10(a and b) shows the Z^* plots for CCTO, LCCTO and LCTO at 120 and 320 K, respectively. It clearly demonstrates that the grain resistance is very high for LCTO, followed by LCCTO and it is much less in the case of CCTO. The smaller resistance of CCTO grains despite their large size (50 μm) indicates that these are more conductive. This may be due to the high tendency of CCTO for oxygen loss during
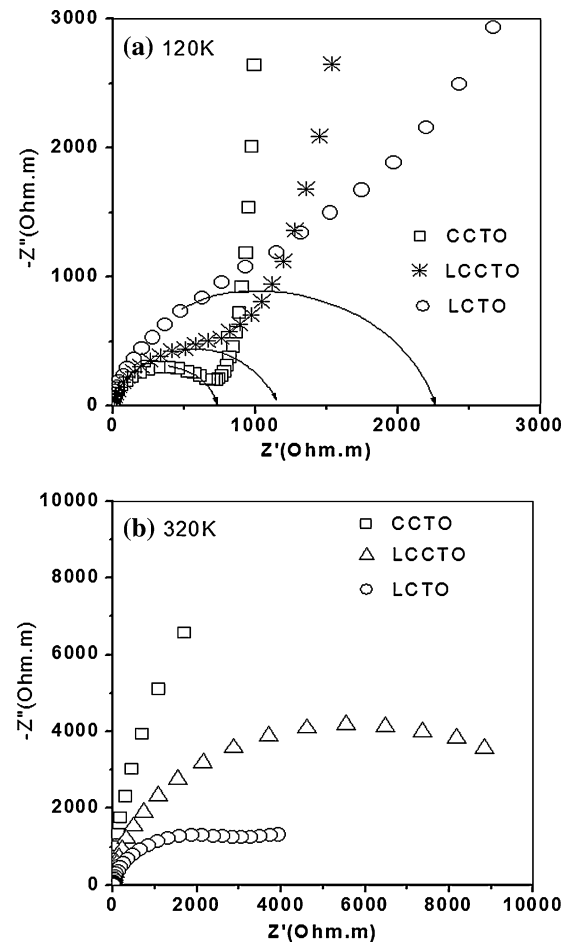

Fig. 10 Impedance complex plane plot, Z^* of CCTO, LCCTO and LCTO ceramics at (**a**) 120 K (grain), (**b**) 320 K (grain boundary)

sintering. The trend is different at 320 K (Fig. 10b). The grain boundary resistance is the highest for CCTO. This is attributed to the presence of secondary phase at the grain boundary.

In Fig. 11, the plot of ratio between grain boundary resistance at 320 K and the grain resistance at 120 K for all the three samples is depicted. It is evident from this figure that this ratio is the highest for CCTO. Thus, the internal barrier layer effect, which depends on the resistivity difference between the grain and grain boundary, is more pronounced in CCTO and consequently higher ε_r' at lower frequencies.

3.4 Complex modulus analysis

The modulus study is an important tool to investigate into the electrical transport process in ceramics and to distinguish the microscopic processes responsible for localized dielectric relaxation [25]. For a system consisting of two electrically active regions such as the
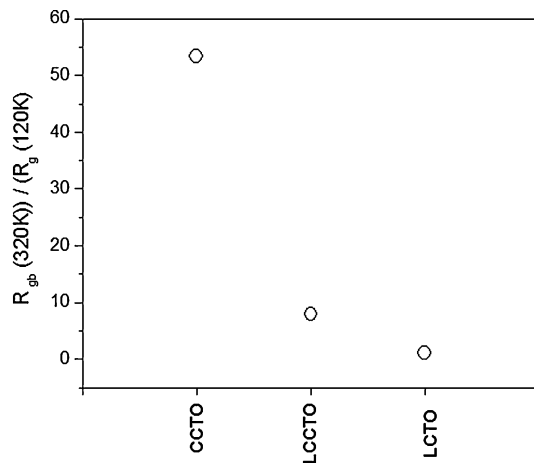
Fig. 11 Ratio of grain boundary resistance at 320 K to grain resistance at 120 K for CCTO, LCCTO and LCTO ceramics

grain and the grain boundary represented by two parallel RC circuits as in the Fig. 6, the imaginary part of the modulus response is given by [26],

$$M'' = \frac{\varepsilon_0}{C_g}\left[\frac{\omega R_g C_g}{1 + (\omega R_g C_g)^2}\right] + \frac{\varepsilon_0}{C_{gb}}\left[\frac{\omega R_{gb} C_{gb}}{1 + (\omega R_{gb} C_{gb})^2}\right]$$

For such a system, the grain and grain boundary response peaks, respectively occur at frequencies $1/(2\pi R_g C_g)$ and $1/(2\pi R_{gb} C_{gb})$. Since, peak values are proportional to the reciprocal of the associated capacitance, the smallest capacitance will dominate in the electric modulus plots. The grains usually have smaller capacitances than the grain boundaries; their peak is stronger in the modulus spectra. Figure 12(a and b) shows the frequency dependence of M'' at different temperatures for LCTO samples. As in the case of impedance formalism, the relaxation peaks of grain and grain boundaries appear in two separate temperature regimes. Strong peaks that appear up to 160 K in the high frequency range (10^4–10^6 Hz) are originating from grains and those from the grain boundaries appear above room temperature. The peaks shift to higher frequencies on increasing temperature. Furthermore, the intensities of the peaks owing to grain response are nearly 20 times greater than those from the grain boundaries. This indicates that capacitance associated with the grains is roughly 20 times smaller than that of the grain boundary. This behavior is similar to that of CCTO.

Figure 13a shows the modulus loss spectra (M'' versus f) of grains for CCTO, LCCTO and LCTO at 120 K and it is clear from the spectra that grain relaxation occurs in the same frequency range for CCTO and LCCTO with a small downward shift in the
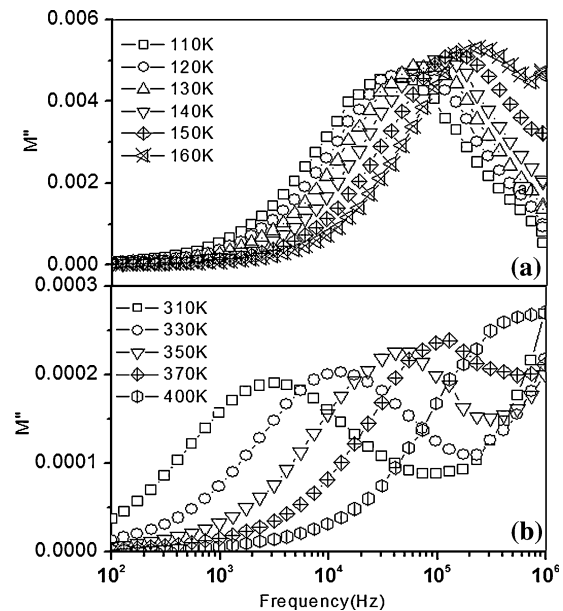

Fig. 12 Frequency dependence of imaginary part (M'') of electric modulus for LCTO ceramics at different temperatures (a) grain, (b) grain boundary

case of LCTO. This implies that relaxation time $\tau = RC$ is nearly the same for all the three compounds. The decrease in peak heights for M'' versus f plots for La^{3+} doped ceramics suggest that the grain capacitance is slightly higher. Since, the difference in capacitance of the three samples is marginal; it is suggestive in a gross way that the true lattice responses of the present compounds remain unaltered despite vast difference in their effective dielectric constants at low frequencies.

The modulus loss spectra of grain boundary for CCTO, LCCTO, and LCTO at 370 K are depicted in Fig. 13b. The magnitude of the M''_{max} increases drastically with increase in the dopant (La^{3+}) concentration and peak height for CCTO is an order of magnitude smaller than that of LCTO. Moreover, grain boundary relaxation does not occur at the same frequency for all three compounds. The $\tau = 1/\omega_{max} = RC$ is highest for CCTO and is the lowest for LCTO. Figure 13c shows the variation of grain boundary capacitance calculated from the modulus height with La^{3+} doping. The grain boundary capacitance decreases sharply with increase in doping level.

Based on the above experimental facts, the observed dielectric behavior of all three compounds under study may be rationalized as follows.

The dielectric response of the equivalent circuit in the Fig. 6 could be presented in the following form [27]

$$\varepsilon^*(\omega) = \varepsilon'_\infty + \frac{\varepsilon'_s - \varepsilon'_\infty}{1 + i\omega\tau} - i\frac{\sigma}{\omega} \tag{1}$$
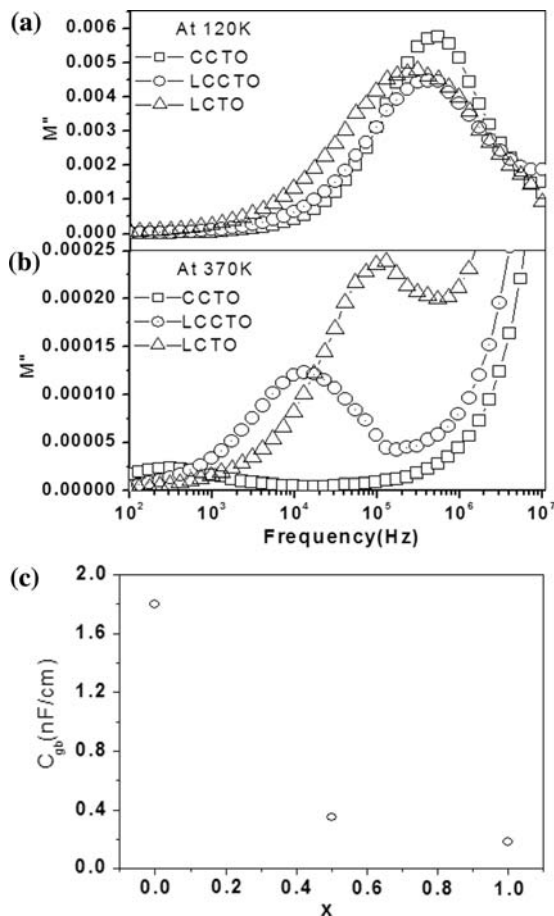
Fig. 13 (a and b) Frequency dependence of imaginary part (M'') of electric modulus for CCTO, LCCTO and LCTO at different temperatures (a) grain, (b) grain boundary, (c) grain boundary capacitance for CCTO, LCCTO and LCTO ceramics at 370 K

where

$$\varepsilon'_{\infty} = \frac{1}{C_0} \left[\frac{1}{\frac{1}{C_g} + \frac{1}{C_{gb}}} \right], \tag{2}$$

$$\varepsilon'_s = \frac{R_g^2 C_g + R_{gb}^2 C_{gb}}{C_0 (R_g + R_{gb})^2}, \tag{3}$$

$$\sigma' = \frac{1}{C_0 (R_g + R_{gb})}, \tag{4}$$

$$\tau = \frac{R_g R_{gb} (C_g + C_{gb})}{R_g + R_{gb}}, \tag{5}$$

where, ε'_s, ε'_{∞} are the static and high frequency dielectric constants, respectively, σ' is Ohmic conductivity, C_0 is empty cell constant and τ is the time constant.

Equation 1 shows that equivalent circuit in Fig. 6 gives a relaxation spectrum similar to that of the Debye relaxation. However, the process involved is called

Maxwell–Wagner type, which often occurs in the heterogeneous system in which the conductivities of two components are different. In the present case such a situation would have arisen due to the conducting grains and resistive grain boundaries.

From the previous sections it is clear that $R_{gb} \gg R_b$ and $C_{gb} > 10 C_g$ for all the three samples. Therefore, the effective dielectric constant of the sample at frequencies much lower than the relaxation frequency is be given by

$$\varepsilon_s = \frac{C_{gb}}{C_0} \tag{6}$$

ε'_s is determined by the ratio between grain boundary capacitance C_{gb} and empty cell capacitance C_0. Since, C_{gb} is very much higher for CCTO than that of LCTO, the low frequency dielectric constant is very high for CCTO.

From Eq. 2 the effective dielectric constant of the sample at frequencies much higher than the relaxation frequency is given by,

$$\varepsilon_{\infty} = \frac{C_g}{C_0} \tag{7}$$

ε'_{∞} is determined only by the ratio between grain capacitance and empty cell capacitance. C_g is almost same for all the three samples under investigation, which accounts for the same dielectric constant value at high frequencies.

Moreover, if it is assumed that the grain and grain boundary form two layer capacitors with a thickness $(d_g + d_{gb})$, where d_g and d_{gb} are the thicknesses of the grain and the boundary layers, respectively, from Eq. 6 one obtains, $\varepsilon'_s \approx \varepsilon_{gb}((d_g + d_{gb})/d_{gb})$, where ε_{gb} is the dielectric constant of the grain boundary layer. Therefore, even a small dielectric constant ε_{gb} can lead to a giant dielectric constant ε'_s, if the ratio $(d_g + d_{gb})/d_{gb}$ is large. Hence, for the two materials with same grain boundary dielectric constant, the effective dielectric constant would be higher for the material with the bigger grain size and smaller grain boundary thickness. In the present study, this ratio for CCTO is almost 10 times larger than LCTO, since grain size in CCTO is 50 μm, which is much higher than that of LCTO (grain size ≈5 μm), eventhough they were sintered under similar conditions. Delectric constant of CCTO ceramic is more than 10 times that of LCTO, which is consistent with its microstructure (grain size). It should be noted that LCTO has about 33% vacancies on A site (Ca^{2+}) site which do not really seem to have a tremendous influence on the dielectric properties as macroscopic parameters are very much dominant.

4 Conclusions

Phase pure $Ca_{(1-x)}La_{(2/3)x}Cu_3Ti_4O_{12}$ ($x = 0$, 0.5, 1) ceramics have been prepared by solid state reaction route. XRD studies indicated the structure of $Ca_{(1-x)}La_{(2/3)x}Cu_3Ti_4O_{12}$ to be cubic structure with a small increase in lattice parameter on doping due to relative size difference between Ca^{2+} and La^{3+}. There is a remarkable decrease in grain size from 50 μm to 3–5 μm in Lanthanum doped ceramics. The dielectric constant of CCTO decreased with increase in La^{3+} doping. The frequency and temperature dependence of all the three samples under study were found to be similar, with the dielectric constant exhibiting Debye type of relaxation. The grain and grain boundary contributions for the electrical characteristics of the samples were separated by impedance and modulus spectroscopy. La^{3+} substitution at the Ca^{2+} site resulted in an increase in the resistance of the grains and a decrease in grain boundary resistance, consequently a decrease in the grain boundary internal barrier layer effect. The observed dielectric behavior of all the three samples were explained based on the Maxwell–Wagner relaxation arising due to the interfaces between grain and the grain boundary.

References

1. M.A. Subramanian, D. Li, N. Duan, B.A. Reisner, A.W. Sleight, J. Solid State Chem. **151**, 323 (2000)
2. B.-G. Kim, S.M. Cho, T.-Y. Kim, H.M. Jang, Phys. Rev. Lett. **86**, 3404 (2001)
3. J. Wu, C.-W. Nan, Y. Lin, Y. Deng, Phys. Rev. Lett. **89**, 217601 (2002)
4. S. Garcia-Martin, A. Morata-Orrantia, M.H. Aguirre, M.A. Alario-Franco, Appl. Phys. Lett. **86**, 43110 (2005)
5. I.P. Raevski, S.A. Prosandeev, A.S. Bogatin, M.A. Malitskaya, L. Jastrabik, J. Appl. Phys. **93**, 4130 (2003)
6. C.C. Homes, T. Vogt, S.M. Shapiro, S. Wakimoto, A.P. Ramirez, Science **293**, 673 (2001)
7. M.A. Subramanian, A.W. Sleight, Solid State Sci. **4**, 347 (2002)
8. D.C. Sinclair, T.B. Adams, F.D. Morrison, A.R. West, Appl. Phys. Lett. **80**, 2153 (2002)
9. T.B. Adams, D.C. Sinclair, A.R. West, Adv. Mater. **14**, 1321 (2002)
10. M.H. Cohen, J.B. Neaton, L. He, D. Vanderbilt, J. Appl. Phys. **94**(1), 3299
11. G. Chiodelli, V. Massarotti, D. Capsoni, M. Bini, C.B. Azzoni, M.C. Mozzati, P. Lupotto, Solid State Commun. **132**, 241 (2004)
12. T.-T. Fang, H.-K. Shiau, J. Am. Ceram. Soc. **87**, 2072 (2004)
13. Z.-J.T. Lei Zhang, Phys. Rev. B **70**, 174306 (2004)
14. G. Zang, J. Zhang, P. Zheng, J. Wang, C. Wang, J. Phys. D Appl. Phys **38**, 1824 (2005)
15. J.L. Zhang, P. Zheng, C.L. Wang, M.L. Zhao, J.C. Li, J.F. Wang, Appl. Phys. Lett. **87**, 142901 (2005)
16. L. Zhang, Appl. Phys. Lett. **87**, 022907 (2005)
17. E.A. Patterson, S. Kwon, C.-C. Huang, D.P. Cann, Appl. Phys. Lett. **87**, 182911 (2005)
18. L. Wu, Y. Zhu, S. Park, S. Shapiro, G. Shirane, J. Tafto, Phys. Rev. B **71**, 14118 (2005)
19. F.D. Morrison, D.C. Sinclair, A.R. West, J. Am Ceram. Soc. **84**, 531 (2001)
20. F.D. Morrison, D.C. Sinclair, A.R. West, J. Am. Ceram. Soc. **84**, 474 (2001)
21. A.R. West, T.B. Adams, F.D. Morrison, D.C. Sinclair, J. Eur. Ceram. Soc. **24**, 1439 (2004)
22. J. Liu, C.-G. Duan, W.N. Mei, R.W. Smith, J.R. Hardy, J. Appl. Phys. **98**, 93703 (2005)
23. B.A. Bender, M.-J. Pan, Mater. Sci. Eng. B **117**, 339 (2005)
24. D.C. Sinclair, A.R. West, J. Appl. Phys. **66**, 3850 (1989)
25. R. Gerhardt, J. Phys. Chem. Solids **55**, 1491 (1994)
26. J. Liu, C.-G. Duan, W.-G. Yin, W.N. Mei, R.W. Smith, J.R. Hardy, J. Chem. Phys. **119**, 2812 (2003)
27. V. Hippel, *Dielectrics and Waves* (Wiley, New York, 1954)